



## Enhanced adsorption of phenol using graphene oxide-bentonite nanocomposites: Synthesis, characterisation, and optimisation

Hassan Wathiq Ayoob<sup>a,b</sup>, Ali M. Ridha<sup>b</sup>, Ala'a Abdulrazaq Jassim<sup>a</sup>, Nabil Kadhim Taieh<sup>b,\*</sup>, Raad Z. Homod<sup>c,\*</sup>, Hayder Ibrahim Mohammed<sup>d</sup>

<sup>a</sup> Dept. of Chemical Engineering, Engineering College, Basra University, Basra, Iraq

<sup>b</sup> Dept. of Materials Engineering Technology, Technical Engineering College-Baghdad, Middle Technical University, Baghdad, Iraq

<sup>c</sup> Department of Oil and Gas Engineering, Basrah University for Oil and Gas, Basra, Iraq

<sup>d</sup> Department of Physics, College of Education, University of Garmian, Kurdistan, Iraq

### ARTICLE INFO

#### Keywords:

Adsorption  
Graphene oxide intercalation  
Bentonite, nanocomposite  
Hummer's method  
Langmuir isotherm

### ABSTRACT

Wastewater treatment is crucial because it causes harm to the environment of human beings. Adsorbents are faulted by low adsorption capacity and difficult recovery due to organic pollutants. This study aims to improve adsorption capacities using bentonite and other environmentally friendly and economically feasible adsorbents. To do this, using Hammer's approach, bentonite was subjected to an acidic treatment (1.5 M H<sub>2</sub>SO<sub>4</sub>) and then hybridized with synthetic graphene oxide (GO). Integrating GO nanosheets within the interlayer of acid-activated bentonite and depositing them onto the exterior surface using a simple ultrasonic-assisted method successfully created a graphene oxide-bentonite nanocomposite. GO, and its composites (at 5 and 10 wt%) were characterized using ATR-FTIR, BET, XRD, FE-SEM, and AFM studies. The results demonstrated that GO with a single-layer thickness of 0.618 nm could be successfully fabricated. We employed energy-dispersive X-ray spectroscopy (EDX) to detect changes in chemical composition before and after phenol adsorption. It was thoroughly studied how essential factors, including adsorbent dosage, pH, agitation period, and beginning phenol concentration, affected adsorption behavior. An obvious increase of the adsorption capacities from 30.69 to 46.43 mg/g were achieved under ideal circumstances of pH 6, an 8-hour contact duration, and doses of 0.3 g and 0.2 g for GO-MB5 and GO-MB10 composites, respectively. The pseudo-second-order kinetic and Langmuir equilibrium isotherm models efficiently described the adsorption process. More notably, the synthesized adsorbents could be successfully regenerated and used without major capacity losses after six cycles. This study highlights the effectiveness of GO-bentonite nanocomposites as effective adsorbents for environmental treatment.

### 1. Introduction

The problem of water shortages has increased all over the world. To solve this issue, wastewater reuse has become an urgent solution—industrial waste is a significant source of different forms of natural water contamination. Wastewater consists mainly of oxygen-demanding materials, grease, oil, scum, pathogenic bacteria, viruses, pesticides, refractory organic compounds, and heavy metals [17]. Phenol has become one of the most abundant organic pollutants in industrial wastewater and is considered by the US Environmental Protection Agency (EPA) as one of the priority pollutants [19]. The phenolic

compounds from different industries, such as petroleum, petrochemical, pharmaceutical, and phenol-producing industries, represent one of the most dangerous contaminants in wastewater because of their high toxicity, even at low concentrations [29]. Most of the abovementioned industries are present in Iraq, particularly in Basra, where I currently reside, and they pollute the water supply. Phenols were selected for this reason. Many approaches for removing phenol from wastewater, such as flocculation, enzymatic, chemical oxidation, biological process, distillation, extraction, zonation, ion exchange, and membrane processes, are available. The drawbacks of these approaches are being expensive, incomplete removal of organic and metals, and hazardous sludge

\* Corresponding authors.

E-mail addresses: [hassan.wathiq@uobasrah.edu.iq](mailto:hassan.wathiq@uobasrah.edu.iq) (H.W. Ayoob), [ali.ridha@mtu.edu.iq](mailto:ali.ridha@mtu.edu.iq) (A.M. Ridha), [alaa.jassim@uobasrah.edu.iq](mailto:alaa.jassim@uobasrah.edu.iq) (A.A. Jassim), [nabeel\\_khadum@mtu.edu.iq](mailto:nabeel_khadum@mtu.edu.iq) (N.K. Taieh), [raadahmood@yahoo.com](mailto:raadahmood@yahoo.com) (R.Z. Homod), [hayder.i.mohammad@garmian.edu.krd](mailto:hayder.i.mohammad@garmian.edu.krd) (H.I. Mohammed).

<https://doi.org/10.1016/j.molliq.2023.123833>

Received 30 August 2023; Received in revised form 25 November 2023; Accepted 18 December 2023

Available online 21 December 2023

0167-7322/© 2023 Elsevier B.V. All rights reserved.

production or other waste products that require adequate disposal. Among these processes, adsorption is considered to be highly effective, cheap, and easy to use [45]. In recent years, the research interest has escalated into making low-cost, eco-friendly adsorbent materials for removing pollutants in wastewater. The adsorbent material must be abundant or a byproduct or waste material [39]. Due to its high surface area, excellent solubility in water, and containing productive, functional groups on its surface, which provide sufficient active sites for adsorption, Graphene oxide (GO) is considered a super adsorbent for water treatment.

Meanwhile, GO is easy to agglomerate, leading to decreases in the active sites, which highly weaken its adsorption ability; therefore, GO composites have drawn increasing interest in the application of water treatment [40]. Bentonite is an aluminum phyllosilicate clay composed mainly of montmorillonite (MMT). In recent years, clay mineral adsorbents, especially Montmorillonite (MMt), have become an alternative to active carbon. Bentonite has the potential to be used as a low-cost sorbent since it is naturally available and has a high surface area. The MMt crystal molecule sandwich structure consists of one alumina octahedral central sheet between tetrahedral silica sheets. The hydrophobicity of the interlayer and the cation exchange of MMt positively affect its adsorption efficiency. The MMt problems are low efficiency and difficulty in simultaneous removal. The combination of GO with MMt eliminates their respective issues. Go-Go-MMt-based materials are now used as adsorbents to manage wastewater for single or binary heavy metal ions and organic contaminants [46].

The nanocomposite was prepared very simply and easily, similar to the following research [41]. However, we increased the vaccination rate significantly compared to what was reported in previous research (10 % instead of 2 %). Iraqi bentonite was also used instead of Chinese bentonite. Here we point out the difference in the proportions of bentonite components as shown in Table 1 [42,33,43,48,2,9] respectively. To our knowledge, no researcher has used this nanocomposite to remove phenol, as shown in Table 2, which makes it a novel approach. The prepared adsorbent represents a new idea of research that is required to investigate using ATR-FTIR, BET, XRD, FE-SEM, XRF, and AFM. as characterization tools.

This study introduces a novel approach by developing the GO-MB nanocomposite and exploring its effectiveness as a phenol adsorbent, demonstrating original contributions to environmentally friendly adsorption. Comprehensive characterization employing X-ray Diffraction (XRD), Attenuated Total Reflectance Infrared Spectroscopy (ATR-FTIR), Field Emission Scanning Electron Microscopy (FE-SEM), and Brunauer-Emmett-Teller (BET) analysis underscores the uniqueness of the synthesized composite adsorbents. The investigation systematically analyzes the impact of process variables on adsorption, including adsorbent dosage, pH, contact time, and adsorbent type. Employing Langmuir, Freundlich, and Temkin adsorption isotherm models enhances the understanding of adsorption equilibrium, while exploration of kinetic models provides insights into adsorption rates. The study's significant contributions lie in introducing the GO-MB nanocomposite as

**Table 1**

Shows the chemical composition and loss of ignition (LOI) of bentonite from different places around the world.

Chemical composition%	Saudi Arabia	Iran	Turkey	China	Nigeria	Algeria	Iraq (This work)
SiO <sub>2</sub>	55.89	64.13	34.9	69.17	52.3	58.32	43.642
Al <sub>2</sub> O <sub>3</sub>	16.03	12.75	9.36	14.43	24.5	15.82	10.716
CaO	3.25	2.38	14.4	1.29	—	0.95	4.8875
Fe <sub>2</sub> O <sub>3</sub>	4.19	4.46	3.21	3.12	10.8	2.63	4.403
MgO	2.75	0.95	7.13	3.31	3.78	3.31	2.558
Na <sub>2</sub> O	0.34	3.17	2.73	1.95	0.96	1.89	0.884
K <sub>2</sub> O	0.49	0.94	2.11	0.83	0.61	1.19	0.467
TiO <sub>2</sub>	0.15	0.46	0.28	0.13	2.56	0.15	0.466
P <sub>2</sub> O <sub>5</sub>	0.086	—	—	—	—	0.11	0.184
SO <sub>3</sub>	0.23	—	0.1	—	—	—	—
LOI	17.2	8.37	22.3	5.40	4.27	13.73	17.35

**Table 2**

Comparison of various adsorbents used to phenol removal from aqueous solutions.

Adsorbent	Adsorption Capacity (mg/g)	Reference
M-bentonite	9.9	[3]
Al-Bentonite	8.7	
CTAB-treated bentonite	8.4	
T-bentonite	8.2	
agro-waste based activated carbon	11.01	[37]
Chitosan	2.22	[21]
Salicylidene-chitosan	8.50	
Cyclodextrin-chitosan	34.93	
cyclodextrin polymer-chitosan	131.50	
powdered activated carbon:		[25]
bamboo charcoal	24.96	
coconut shell charcoal	21.22	
coal charcoal	20.14	
Ca-bentonite/chitosan composite	12.496	[30]
Graphene oxide nanosheet suspensions	1000	[45]
Single walled carbon nanotubes (SWCN)	19.898	[20]
	21.163	
Single walled carbon nanotubes after oxidation (SWCNO)	17.948	
	16.276	
Multiwalled carbon nanotubes (MWCNT)	16.316	
	22.781	
Multiwalled carbon nanotubes after oxidation (MWCNTO)		
Riduced Grappene oxide (RGO)		
Grappene oxide (GO)		
Graphene oxide nanoflak	19–30 (for emerging and common phenolic compounds)	[10]
Free and immobilized nano peroxidase particles	—	[29]
Starch hybrid hydrogels (Polyacrylamide)	21	[12]
graphene oxide nanoparticles hybrid-UV irradiation process.	—	[4]
GO-MB5	30.69	This work
GO-MB10	46.43	

a promising adsorbent and the detailed elucidation of its adsorption behavior and mechanisms, marking advancements in environmentally sustainable adsorption practices and practical applications.

## 2. Materials and methods

### 2.1. Materials

The natural bentonite rock was sourced from the Iraqi National Company for Geological Survey and Mining in Baghdad, Iraq. Necessary chemicals were purchased from Areej Al-Furat Co, Ltd in Iraq, including graphite powder, phenol (C<sub>6</sub>H<sub>5</sub>OH), sodium nitrate (NaNO<sub>3</sub>), sulfuric acid (H<sub>2</sub>SO<sub>4</sub>, 98 %), hydrochloric acid (HCl, 37 %), potassium permanganate (KMnO<sub>4</sub>), hydrogen peroxide (H<sub>2</sub>O<sub>2</sub>, 30 %), and sodium oxide (NaOH). For the creation of all solutions, only distilled water was

utilized.

## 2.2. Synthesis of graphene Oxide(GO)

Using Hummer's method, graphene oxide was prepared from natural graphite powder [16]. The graphite powder (5 g) and  $\text{NaNO}_3$  (2.5 g) were mixed with concentrated  $\text{H}_2\text{SO}_4$  (98 %, 115 ml) and stirred for 30 min by a magnetic stirrer. Then, the potassium permanganate (15 g) was added slowly to the mixture in a 15–20 min period with continuous stirring in an ice bath at a temperature (of 0–10 °C). The mixture was then transferred to a water bath at (35–40 °C) and stirred for 30 min. Distilled water (230 ml) was then added drop-wise with stirring. The mixture was then transferred to a water bath at 90 °C and stirred for 15 min. 700 ml of distilled water was added slowly to the mix with stirring. The reaction was then terminated by adding 50 ml hydrogen peroxide ( $\text{H}_2\text{O}_2$  30 %) and stirring the mixture for one hour. This research uses a new washing process instead of filtration or centrifuge. After the graphite oxidation reaction terminated, distilled water was added and left the solution to settle down; then, water was drawn out, and the precipitate was left at the bottom of the beaker, repeated many times. Then, the precipitate was dried at 50–60 °C for 24 hrs, grounded, washed with 100 ml dilute HCl (10 % by volume), stirred for 10 min, and dried again to gate granular graphite oxide. The graphite oxide powder was dispersed in distilled water (0.5 mg/ml) using ultra-sonication to obtain graphene oxide (GO).

## 2.3. Acid treatment of bentonite

The as-received bentonite was crushed, washed with distilled water several times until it became without impurities, dried at 70 °C, and then sieved to a particle size  $75 \times 10^{-6}$ , including 200 grid using a Raw Bentonite (RB). Raw bentonite was then activated using 1.5 M (molarity)  $\text{H}_2\text{SO}_4$  at a fixed acid-to-clay ratio is 1:10. The solution was then mixed using magnetic stirring for 3 h, washed many times with distilled water to obtain a pH value of 7, filtration and then bentonite has dried at 70 °C for 3 h, which, called activated bentonite (MB).

## 2.4. Preparation of graphene oxide-bentonite composite (GO-MB)

Activated bentonite powder and various graphene oxide (GO) loadings at 5 and 10 wt% were carefully combined with distilled water. This mixture underwent 3 h of ultrasonic treatment in a flask, followed by another 30 min of stirring in a water bath with a constant temperature of 90 °C. The composite material was then separated from the resulting amalgam using filtering and heated to a regulated temperature of 60 °C for 24 h. The remaining material in the flasks underwent a cooling phase after the drying process was finished before being painstakingly pulverized to attain the necessary consistency and morphology for experimental use. This organized process ensures that the graphene oxide-bentonite nanocomposite is prepared thoroughly and consistently, providing the groundwork for further research and analysis.

## 2.5. Characterisation

An attenuated Total Reflection Fourier Transform Infrared (ATR-FTIR) Spectrometer was used to observe changes in the organic compound group recorded on (IRAffinity-1, Shimadzu Co., Japan). The crystalline powder phase was determined using X-ray Diffractometry (XRD-6000, Shimadzu Co., Japan) using  $\text{Cu-K}\alpha$  radiation ( $\lambda = 1.5418 \text{ \AA}$ ). The morphology and structure were characterized by a Field emission scanning electron microscope (FE-SEM) and were examined by (ZEISS Gemini SEM 560). Brunauer-Emmett-Teller (BET) and Barrett-Joyner-Halenda (BJH)(model: 9600, USA) techniques were utilized for the calculation of surface area, pore volume, and pore diameter for the adsorbents. The thickness and morphology of prepared graphene oxide were determined by Atomic Force Microscopy (Ntegra Prima, NT-MDT

Spectrum Instruments Co., Russia). The absorbance value of phenol in solution was determined using a UV-vis spectrophotometer (Uv-1100, EMCLAB, Germany) to calculate the phenol concentration.

## 2.6. Batch adsorption for removal of phenol

Batch experiments were conducted to investigate the adsorption characteristics of phenol onto GO-MB5 and GO-MB10 nanocomposites, which were performed at 25 °C on a rotary shaker water bath (ST 402, NÜVE, Turkey) at 120 rpm. The effect of operating variables such as adsorbent dosage ranging from 0.1 to 1.2 g weighted by calibrated four digits digital balance (ABS 220-4, sensitivity  $\pm 0.0001\text{gm}$ , DENVER, Germany) and the solution pH value range of (2–10) were studied using Mi150pH Meter (Martini, Romania). Adsorption kinetics have been carried out for the time range (2–16 hrs.). Adsorption isotherms were studied at different phenol concentrations (25–200 mg/L) prepared using volumetric flasks. The equilibrium solution was centrifuged by HERMLE Labortechnik (GmbH, Z32HK, Germany) at a speed of 10,000 rpm for 30 min and filtered using a syringe filter of 0.22  $\mu\text{m}$ , and the remaining concentration was determined by Uv-1100, EMCLAB, Germany, at a wavelength of 271 nm. All the adsorption experiments had been repeated three times, and their average was reported [24]. The relative standard deviation values for adsorption isotherms and kinetics were less than 5 %. The adsorbed amount of phenol and removal efficiency can be determined by the following equations [35]:

$$q_e = \frac{(C_o - C_e) \times V}{m} \quad (1)$$

$$R(\%) = \frac{C_o - C_e}{C_o} \times 100 \quad (2)$$

where  $q_e$  (mg/g) is the amount of phenol adsorbed onto GO-MB5 and GO-MB10;  $C_o$  and  $C_e$  (mg/mL) are the initial and equilibrium concentration of phenol, respectively;  $V$  (mL) is the volume of solution;  $m$  (g) is the mass of adsorbent; and  $R$  (%) is the removal percentage of phenol.

## 3. Result and discussion

### 3.1. Structural and characterization of materials

Through X-ray diffraction (XRD) examination, Fig. 1a shows the unique stacking order importance of the graphite and graphene oxide diffraction peaks. The layered carbon structure of graphite is revealed by a distinctive rise in the XRD pattern at  $2\theta = \sim 26.38^\circ$  that corresponds to an interlayer distance ( $d$ ) of 0.337 nm (3.37  $\text{\AA}$ ). A new peak replaces the sharp graphite peak at  $2\theta = \sim 10.94^\circ$  and an interlayer distance of 0.808 nm (8.08  $\text{\AA}$ ) after oxidation into graphene oxide. The stacked layers of graphite are replaced by more dispersed layers in graphene oxide, highlighting structural changes and the effects of oxidation on the material's atomic structure. The XRD study captures the conversion from graphite to graphene oxide, emphasizing interlayer spacing and stacking differences. According to [41], the observed disappearance of the peak at around  $26.38^\circ$  in the X-ray diffraction (XRD) pattern denotes the complete conversion of graphite to graphene oxide nanosheets. This modification is closely related to the structural development brought on by the oxidation process. The noticeable expansion of the interlayer spacing, from 0.337 to 0.808 nm, is a direct result of the oxidation process' addition of oxygen functional groups to the bulk graphite structure's internal and external surfaces. This mechanism causes the stacking order of the graphene oxide sheets to relax, as explained by Ansari et al. in 2017 [7] and Pham et al. in 2011 [32].

Significant structural insights are revealed by analyzing the three different curves in Fig. 1b, which stand for modified bentonite (MB), modified bentonite with 5 % graphene oxide (GO-MB5), and modified bentonite with 10 % graphene oxide (GO-MB10). The peaks detected at a diffraction angle of  $12.0^\circ$  are specifically associated with gypsum,

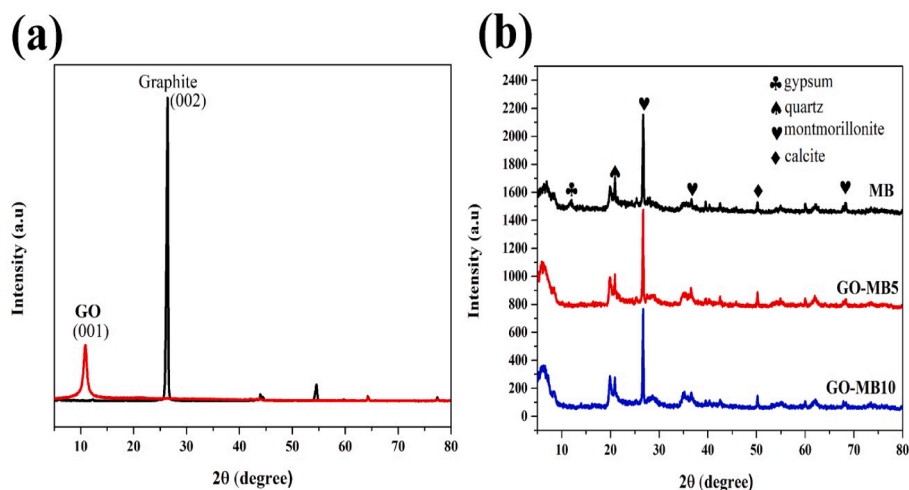


Fig. 1. X-ray diffraction for: (a) graphite and GO, (b) MB, GO-MB5 and GO-MB10.

whereas those at  $20.8^\circ$  are related to quartz. Furthermore, the peaks seen at  $26.5^\circ$ ,  $36.6^\circ$ , and  $68.3^\circ$  correspond precisely to the typical angles of montmorillonite. A peak at  $50.1^\circ$  is indicative of the presence of calcite. The XRD patterns exhibit a strong resemblance to the reference patterns specified in the standard JCPDS files (card no. 01-088-0891 and 00-003-0418) and are consistent with the findings reported by [38,5]. Remarkably, the peak undergoes a gradual shift from  $2\theta = 6.35^\circ$  to  $5.90^\circ$  for GO-MB5 and  $5.60^\circ$  for GO-MB10 with an increasing concentration of graphene oxide in the modified bentonite. This observed shift indicates that the introduction of graphene oxide during the modification process results in the forming of an exfoliated structure. Bragg's law, expressed as  $\lambda = 2d \sin\theta$ , provides additional insight into this evolutionary change in structure. Examining the correlation between the diffraction angle and layer spacing ( $d$ ), it becomes apparent that the layer spacing for GO-MB5 and GO-MB10 has expanded from 1.39 nm in the modified bentonite to 1.50 nm and 1.58 nm, respectively. This expansion indicates the successful integration of graphene oxide into the bentonite structure, leading to an increased layer gap. These research findings, documented by Liu et al. in 2018 [22], elucidate how the structural dynamics shift upon adding graphene oxide. They support the notion that the incorporation of GO induces a transformation in the layered

structure of bentonite, transitioning it into an exfoliated form.

The functional groups present in graphite and the following modifications upon oxidation to generate graphene oxide (GO) are described in detail by the ATR-FTIR spectrum analysis, as shown in Fig. 2. Graphite's essentially inert nature is highlighted by the absence of distinctive peaks in its first spectra for oxygen functional groups. However, the resulting GO spectrum shows recognizable characteristic peaks after adding an oxidizing agent. Peaks at  $2322.29$  and  $2353.16 \text{ cm}^{-1}$  correspond to the stretching vibrations of carbon dioxide ( $\text{O}=\text{C}=\text{O}$ ) bonds, whereas peaks at  $3606.89$  and  $3738.05 \text{ cm}^{-1}$  indicate the existence of hydroxyl groups ( $\text{O}-\text{H}$ ). While the peaks at  $1531.48$  and  $1639.49 \text{ cm}^{-1}$  are attributable to aromatic bonds ( $\text{C}=\text{C}$ ), the peak at  $1743.65 \text{ cm}^{-1}$  denotes carboxyl groups ( $\text{C}=\text{O}$ ). According to studies by Abdel-Ghani, El-Chaghaby, and Helal in 2015 [1], Liu et al. in 2018 [22], and Gholampour et al. in 2017 [15], an extra peak at  $1033.85 \text{ cm}^{-1}$  denotes the presence of epoxy groups. The study of composite skeleton diagrams indicates spectrum bands between  $1200$  and  $3600 \text{ cm}^{-1}$  that resemble the spectrum bands of graphene oxide and bands between  $450$  and  $1100 \text{ cm}^{-1}$  similar to activated bentonite. This relationship shows that graphene oxide was successfully incorporated into the activated bentonite structure, which is consistent with the findings

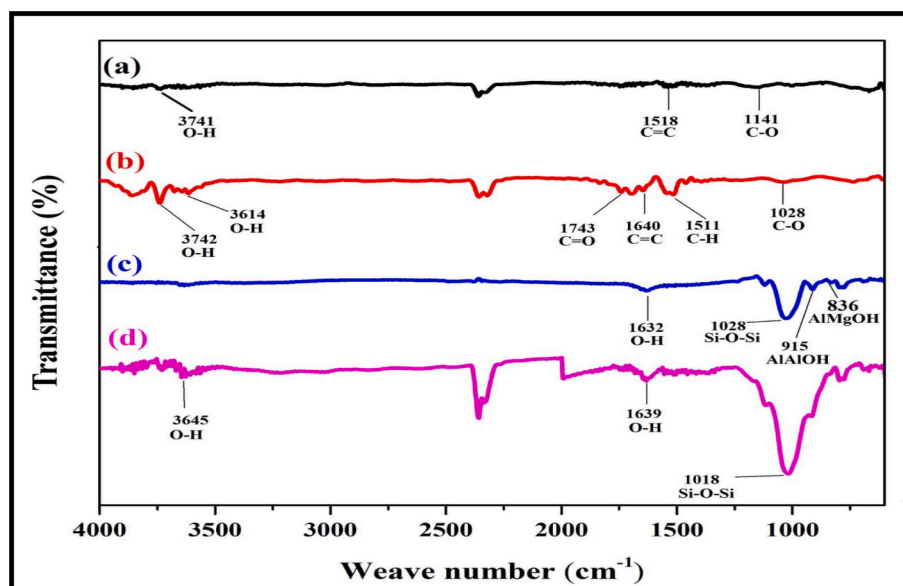


Fig. 2. ATR-FTIR of (a) graphite, (b) GO, (c) MB, (d) GO-MB composite.

of Gholampour et al. in 2017 [15] and Liu et al. in 2018 [22]. Together, these results show how graphite is converted into graphene oxide, distinguished by the appearance of different oxygen functional groups and their successful incorporation into the matrix of activated bentonite, substantiating the structural changes brought on by the oxidation process and the formation of the composite.

Through careful FE-SEM analysis, bentonite's surface morphology and structural changes were studied before and after modifications. Fig. 3a shows graphene oxide (GO) sheets with distinctive surface wrinkling that is consistent with other GO morphological characteristics [8]. Pure bentonite is seen in Fig. 3b as rock-like macroparticles with tightly compressed surfaces. Fig. 3c shows how the surface of bentonite changes after acid alteration, becoming noticeably rougher, more open, and more prone to pinholes [23,36]. Fig. 3d shows that the composite surface shows long-width microcracks and fragile plates after being modified with graphene oxide. Including graphene oxide in the bentonite layers, which caused their exfoliation and the formation of the observed patterns, is closely linked to these structural alterations [40]. Thus, the FE-SEM analyses offer a visual representation of the process, showing how the surface properties change from compacted rock-like structures to open and rough surfaces upon acid modification and eventually to a composite with microcracks and thin plates as a result of the intercalation of graphene oxide. This thorough analysis highlights the significant impact of modification techniques on bentonite's surface morphology and structural makeup, establishing a direct link between the modifications and the resulting alterations in surface characteristics and structural properties.

Our work used energy-dispersive X-ray spectroscopy (EDX) to analyze elements. It enabled us to identify changes in the chemical composition both before and after phenol adsorption. The main objective was to investigate the impact of including graphene oxide at concentrations of 5 wt% and 10 wt% on the adsorption abilities of the nanocomposites. Fig. 4a shows the atomic weight percentages of C, O, Fe, Al, Mg, Ca, and Si before phenol adsorption on GO-MB5. These percentages were 16.23 %, 54.68 %, 1.96 %, 6.11, 1.83, 2.21, and 17.22 %, respectively. After the adsorption of phenol (as shown in Fig. 4b), the atomic percentages for carbon (C), oxygen (O), iron (Fe), aluminum (Al), magnesium (Mg), calcium (Ca), and silicon (Si) changed to 13.02, 57.47, 1.68, 6.15, 1.66, 1.98, and 17.82, respectively. Significantly,

there was a clear rise in the oxygen concentration from 54.68 to 57.47 %. The increase in oxygen concentration may be ascribed to the oxygen present in the chemical composition of phenol, which undergoes a reaction with the surface of GO-MB5. Fig. 5a demonstrates that before phenol adsorption on GO-MB10, the atomic weight percentages of C, O, Fe, Al, Mg, Ca, and Si were 18.42, 54.69, 0.69, 4.66, 0.99, 0.18, and 20.09 %, respectively. After the adsorption of phenol (as shown in Fig. 2b), the atomic percentages for (C), (O), (Fe), (Al), (Mg), (Ca), and (Si) changed to 23.16, 50.45, 0.77, 4.09, 0.86, 0.01, and 20.64 %, respectively. Significantly, there was a noticeable rise in the carbon content, which increased from 18.42 to 23.16 %. The increase in carbon content can be attributed to the carbon present in the chemical composition of phenol, which reacts with the surface of GO-MB10. The rise in oxygen content in GO-MB5 and carbon content in GO-MB10 following phenol adsorption may be ascribed to the chemical interactions between the phenol molecules and the surfaces of these nanocomposites. Phenol possesses oxygen within its structure, and the observed variations in elemental composition indicate the interaction between phenol and the nanocomposite surfaces, resulting in modifications in the atomic proportions of particular elements.

Upon comparing Fig. 4a with Fig. 5a, it becomes evident that there is a decline in the atomic percentages of components Fe, Al, Mg, Ca, and Si as the graphene oxide concentration grows from 5 to 10 %. The decrease in atomic percentages can be attributed to many mechanisms related to incorporating graphene oxide into bentonite. The addition of graphene oxide can create a surface coating that surrounds the bentonite particles, leading to a decrease in the exposure of other elements during Energy Dispersive X-ray Spectroscopy (EDX) measurement. Moreover, the oxygen-containing functional groups found in graphene oxide can chemically interact with the bentonite surface, resulting in modifications to the binding states of certain elements. The arrangement of graphene oxide in layers may affect the ability of the EDX beam to reach the elements behind it in bentonite, thereby impacting the measured atomic percentages. The possible adsorption of contaminants on the surface of bentonite may have further effects on the measured elemental proportions.

Compared to activated bentonite, the composites' BET surface area and pore volume significantly improve (Table 2). This improvement is mainly attributable to adding graphene oxide (GO), which creates an

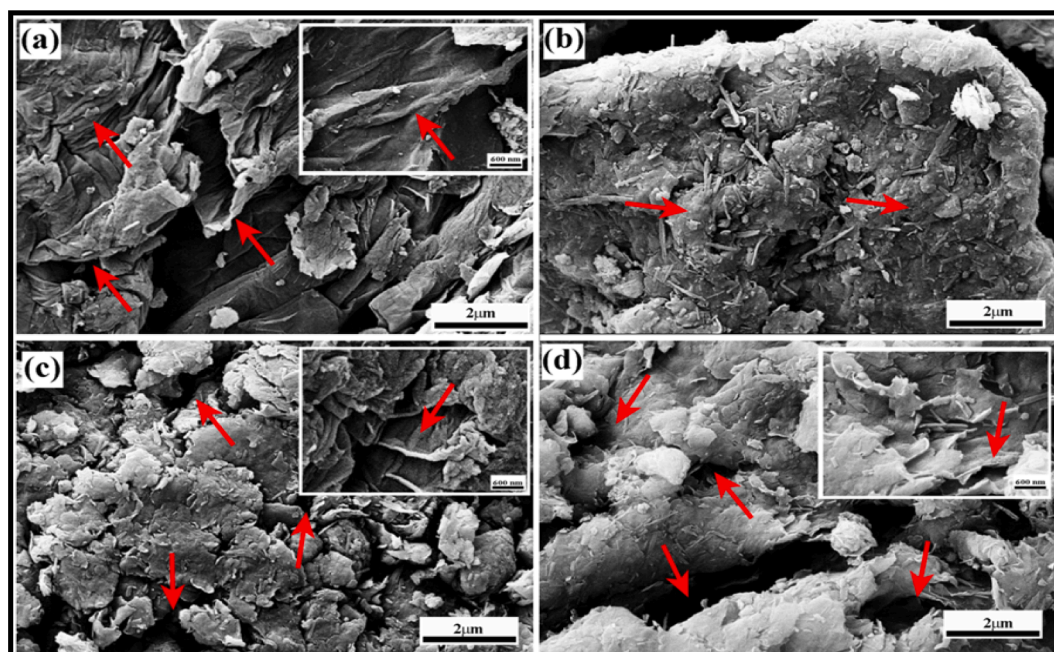


Fig. 3. FE-SEM images of bentonite modified by acid and graphene oxide (GO) (a) GO, (b) pure bentonite, (c) acidified bentonite (MB) and (d) GO-MB5 composite.

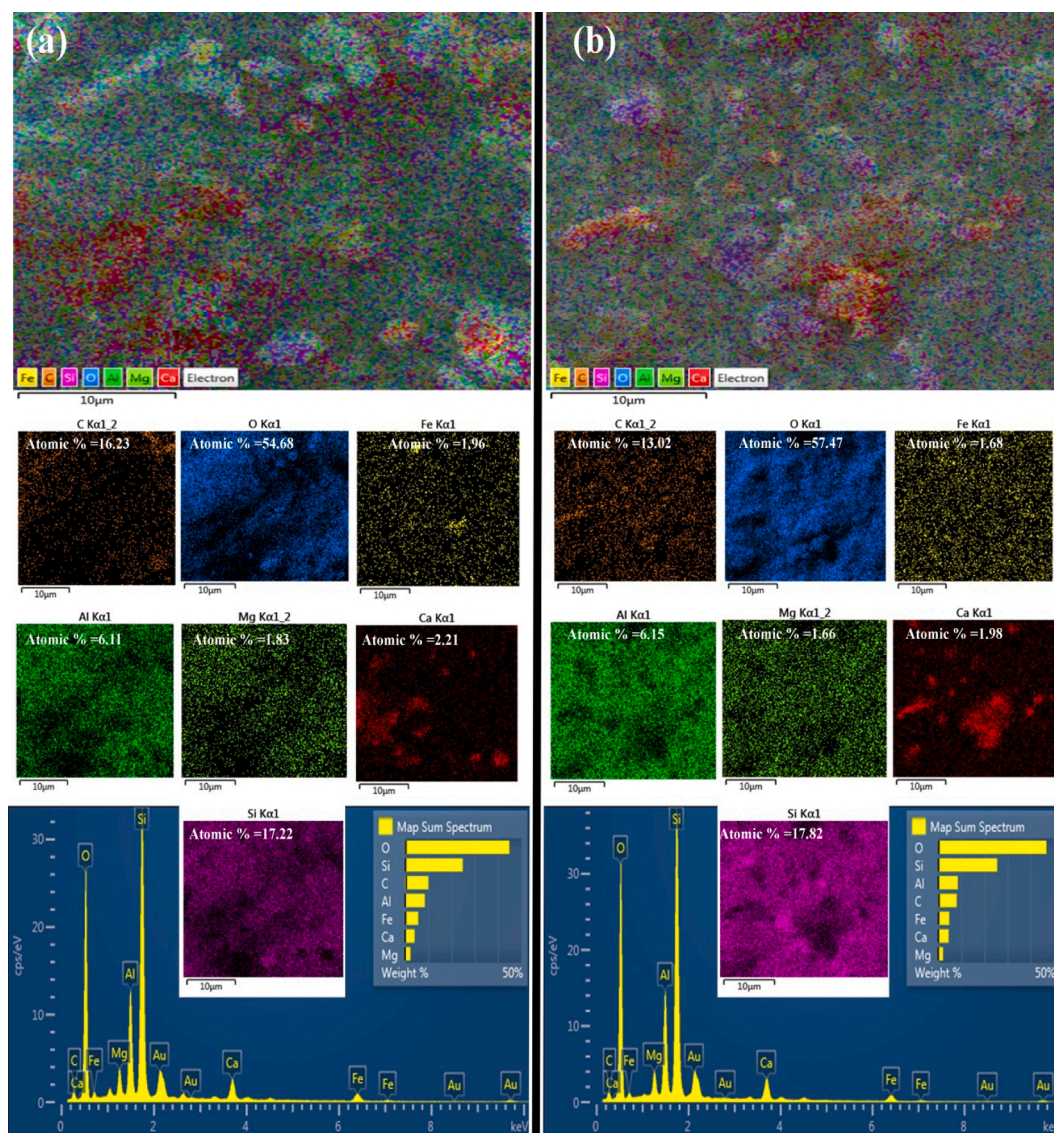


Fig. 4. Energy Dispersive X-ray Spectroscopy (EDX) for GO-MB5. (a) before phenol Adsorption, and (b) after phenol Adsorption.

exfoliated structure as the percentage of GO rises from 5 to 10 wt%, this impact becomes more prominent [41]. The surface area of the composite materials significantly increases when compared to GO itself, growing from 26.375 to 163.026 m<sup>2</sup>/g for GO-MB5 and further to 184.312 m<sup>2</sup>/g for GO-MB10. This increase can be explained by the fact that the measured amount of GO in powder form has a much smaller surface area than the amount of GO used to make the composites, which was dispersed in water [28,47]. Additionally, the composites' decreased pore width indicates the emergence of more active sites, resulting in enlarged pore volume and surface area [26]. This increase in surface area and pore volume illustrates the transformational effect of GO addition and highlights the connection between material composition, structural qualities, and the surface properties that arise.

Atomic force microscopy (AFM) was used to measure the exfoliation levels and provide information on the structural characteristics of graphene oxide (GO). The AFM scans offer a thorough three-dimensional portrayal of GO's topography, making quantifying and characterizing its features easier. The study of GO layers made from graphite oxide, as shown in Fig. 4, indicates a thickness of 0.618 nm and a lateral dimension of 70.6 nm. These results are consistent with earlier work by Galindo et al. from 2014 [14], when it was determined that a few graphene layers had a thickness of between 1 and 2 nm and that a single

layer had a thickness of less than 1 nm. The findings of this investigation unmistakably lead to the creation of a single layer of GO in light of these data. This comprehensive assessment, made possible by the use of AFM, highlights how precisely the layering and thickness characteristics of GO can be determined, proving that a single-layer structure can be successfully achieved in this situation.

### 3.2. Optimisation of the adsorption conditions

Detecting optimal adsorption conditions is essential for removing phenol to provide a cost-efficient adsorption system. The effects of several factors were considered, including the adsorbent dose, the initial pH value, contact time, and the initial concentration of phenol. Different dosages ranging from 0.1 to 1.2 g of each adsorbent (GO-MB5 and GO-MB10) were added to 50 ml of the phenol solution at pH value 7 at 25 °C and 100 mg.L<sup>-1</sup> as an initial concentration for 8 h. agitation time and 120 rpm shaking speed. The adsorption efficiency of phenol is increased with the increase of the adsorbent dosage. It varied from 67.55 and 81.208 % to 99.531 and 99.926 % for GO-MB5 and GO-MB10, respectively. The reason for an increase in adsorption efficiency is due to the greater availability of the surface area of higher concentration of the adsorbent and the complete utilization of all active sites in the adsorbent

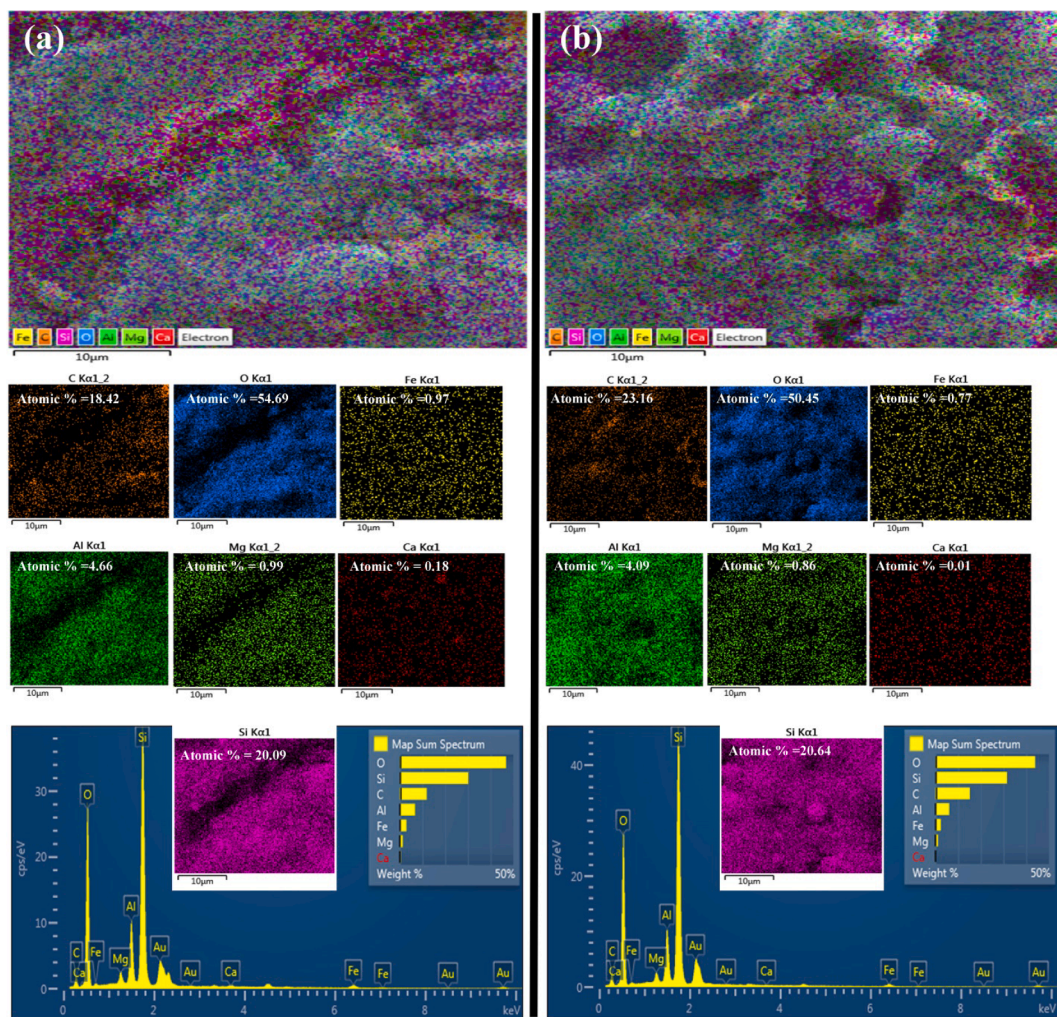


Fig. 5. Energy Dispersive X-ray Spectroscopy (EDX) for GO-MB10. (a) before phenol Adsorption, and (b) after phenol Adsorption.

dosage by phenol ions [30]. The increase in adsorbent dosages after 300 mg for GO-MB5 and 200 mg for GO-MB10 has no significant effect on the removal efficiency due to the equilibrium state between the adsorbent (solid) and adsorbate (liquid). This is because every adsorbent has a limited number of active binding sites, which becomes harder to occupy with the phenol with time. Therefore, adsorbent dosages of 300 and 200 mg were chosen as the optimum dosage to obtain maximum adsorption efficiencies of phenol 96.189 % and 97.926 % for GO-MB5 and GO-MB10, respectively, as shown in Fig. 5a.

To investigate the effect of pH value on the phenol removal percentage, the pH of the phenol solution was varied from 2, 4, 6, 8, to 10. The pH effect of phenol solution on the adsorption efficiencies for GO-MB5 and GO-MB10 is shown in Fig. 5b. These experiments were conducted at the optimum adsorbent dosages. The removal efficiencies of phenol have increased as the pH value increases from 2 to 6, with the maximum removal efficiency of 97.284 and 98.723 % for GO-MB5 and GO-MB10 at a pH value of 6. This might be related to graphene oxide and the interlayer hydrophobicity of bentonite [46]. In contrast, the removal efficiencies decreased at pH > 6. An electrostatic interaction occurs between  $\text{Ca}^{2+}$  on bentonite and phenolate; the acidic pH can offer more adsorption sites on the composite for phenol removal than the alkaline pH [30].

As described in work by Wei et al. in 2020 [40], numerous kinetic models were used to thoroughly analyze the adsorption rate and pinpoint the rate-limiting phase, including the Pseudo first-order (PFO) and second-order (PSO), Elovich (Elo), and Intraparticle Diffusion (IPD)

models. Equation (3) can numerically describe the PFO kinetic model's hypothesis that the rate of adsorption site occupancies is proportional to the number of vacant sites. This method, which Rojas et al. described in 2019 [34], is especially helpful in studying the occupancy dynamics of adsorption sites. Additionally, as explained by [18], the linear formulation of the PFO model is dependent on the adsorption capacity of the adsorbent and can be represented by equation (4). Together, these kinetic models offer essential insights into the kinetics of the adsorption process, making it possible to identify the rate-limiting steps and provide a thorough understanding of the adsorption mechanisms within the context of the investigated materials and systems.

$$qt = qe(1 - e^{-k_1t}) \quad (3)$$

$$\ln(qe - qt) = \ln qe - k_1t \quad (4)$$

The application of the pseudo-second-order (PSO) model in the field of adsorption kinetics presupposes a link between the rate of adsorption site occupation and the square of the active adsorption sites that is expressed by equation (5) in the work of Rojas et al. in 2019 [34]. This model offers useful explanations for how adsorption sites fill up over time. According to [45] description, the equation regulating the PSO model is based on the solid phase's adsorption capacity, and its linear format can be expressed as equation (6). By creating a link between the kinetics rate and the availability of active sites, this model offers a distinctive perspective on the kinetics of adsorption, further enhancing the understanding of the adsorption mechanisms and their associated

dynamics within the examined system.

$$qt = qe \left( 1 - \frac{1}{1 + k_2 t} \right) \quad (5)$$

$$\frac{t}{qt} = \frac{1}{k_2 qe^2} + \frac{t}{qe} \quad (6)$$

The Elovich model is a popular tool for characterizing adsorption processes and is particularly noteworthy for its capacity to explain situations in which the adsorbate persists on the solid surface without passing through desorption. According to this model, the adsorption rate decreases as the amount of time the adsorbate and adsorbent are in contact grows. This occurrence is ascribed to the increasing surface coverage with time. This idea was expanded upon by De La Luz-Asunción et al. in 2015 [20], highlighting the crucial part played by the Elovich model in clarifying the intricate nature of adsorption mechanisms. This model provides essential insights into the dynamic nature of adsorption processes by assuming a continual build-up of adsorbate on the solid surface. It also sheds light on how the surface interactions change as the system develops. The nonlinear and linear Elovich kinetic model equations are expressed by [18]:

$$q_t = \beta \ln(\alpha \beta t) \quad (7)$$

$$qt = 1/\beta \ln(\alpha \beta) + 1/\beta \ln(t) \quad (8)$$

where  $qt$  is the quantity of adsorbate adsorbed at time  $t$  (mg/g),  $k_1$  ( $\text{min}^{-1}$ ) is the pseudo-first-order rate constant,  $K_2$  (mg/g/min) is the pseudo-second-order adsorption constant,  $\alpha$  is a constant related to chemisorption rate and  $\beta$  is a constant which depicts the extent of surface coverage.

The Intraparticle Diffusion model is used to investigate the diffusion-controlled adsorption system. A linear fit indicates that the adsorption process includes the diffusion of two or more steps. Intraparticle Diffusion is the only rate-limiting step if the plot line passes through the origin point. The Weber-Morris model equation is expressed in the following form [34]:

$$q_t = k_{id} t^{1/2} + \theta \quad (9)$$

where  $k_{id}$  is the intraparticle diffusion rate constant ( $\text{mg/g min}^{1/2}$ ),  $\theta$  is a constant that indicates the thickness of the boundary layer (mg/g).

Plotting the adsorption capacity, which is the mass of adsorbed phenol per unit mass of the adsorbent, versus the agitation time ( $t$ ) is required to illustrate the adsorption kinetic curves for phenol onto each adsorbent. This is shown graphically in Fig. 6; through the use of the experimental information, which is rigorously documented in Table 2, linear equations (4), 6, 8, and 9) are used to obtain the characteristic parameters of each kinetic model and adsorbent. This research reveals an intriguing trend: the correlation coefficients ( $R^2$ ) for the composites associated with the pseudo-second-order kinetic model significantly outperform those obtained using other kinetic models. This finding is

significant because the  $R^2$  values quantitatively measure how closely the theoretical models match the experimental results. This comparative investigation highlights the pseudo-second-order kinetic model's improved ability to predict the phenol adsorption kinetics of the investigated adsorbents. The enhanced accuracy and dependability of kinetic interpretations result from the higher  $R^2$  values attained by this model, indicating a tighter agreement between the model's predictions and the experimental results. This thorough analysis helps decipher the temporal dynamics of phenol adsorption and choose the best kinetic model to account for and forecast the complex adsorption behavior of the tested adsorbents.

Describing adsorption isotherm curves for phenol onto each adsorbent involves plotting adsorption capacity ( $q$ ) against the residual concentration of phenol ( $C_e$ ). This graphical representation facilitates the correlation of experimental phenol adsorption data with three prominent theoretical adsorption isotherm models—Langmuir, Freundlich, and Tempkin—as illustrated in Fig. 7. The Langmuir isotherm model, one of the fundamental models in adsorption science, postulates the formation of a monolayer of adsorbate on a homogeneous adsorbent surface [6]. This model is encapsulated by equations (3) and (4), as elucidated by Inyinbor, Adekola, and Olatunji in 2016 [18]. By utilizing the Langmuir isotherm, researchers aim to gain insights into the surface properties of the adsorbent and the interaction between adsorbate molecules and available sites. The juxtaposition of experimental data with these theoretical models empowers researchers to discern the closest fit, revealing which isotherm best describes the adsorption process under investigation [27]. This comprehensive analysis provides a means to characterize the adsorption mechanism and furthers the understanding of the relationship between adsorbent surfaces and adsorbate molecules, offering a robust framework for future optimization and application of adsorption processes (see Fig. 8 and Fig. 9).

$$q_e = (Q \times K_L \times C_e)/(1 + K_L C_e) \quad (10)$$

$$C_e/q_e = C_e/Q + 1/(Q \times K_L) \quad (11)$$

$Q_0$  is the maximum monolayer coverage and capacity (mg/g),  $K_L$  is the Langmuir isotherm constant (L/mg).

The Freundlich isotherm model is an example of an empirical strategy that extends the restriction of representing monolayer coverage alone and broadens its use to multilayer adsorption processes [31]. This model works particularly well for adsorption scenarios on heterogeneous surfaces when active sites' distribution and related energy are exponential. The link between the amount of adsorbate adsorbed and its equilibrium concentration within the adsorbent is captured by Rojas et al. in 2019 [34] in the mathematical expression of the Freundlich isotherm. The adaptability of this empirical model in accommodating multilayer adsorption highlights its use in representing actual adsorption systems where many adsorbate molecules might assemble on the surface of the adsorbent. The Freundlich isotherm contributes to a deeper analytical understanding of adsorption behavior in complex, heterogeneous environments by considering the distribution of active

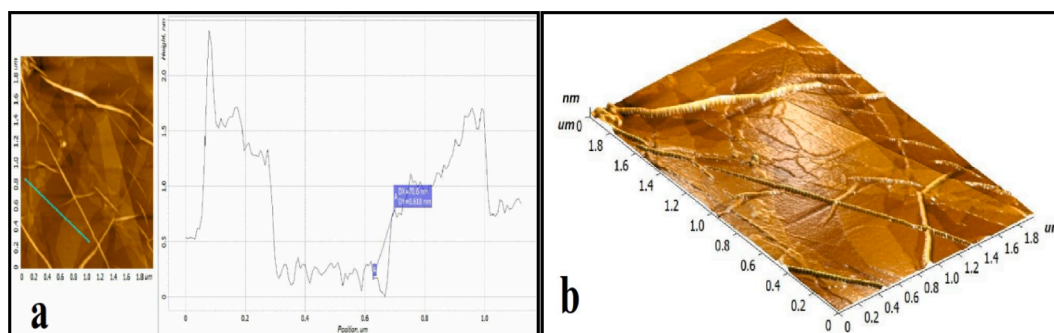


Fig. 6. AFM of graphene oxide (GO), (a) thickness and lateral size, and (b) 3-D topography.

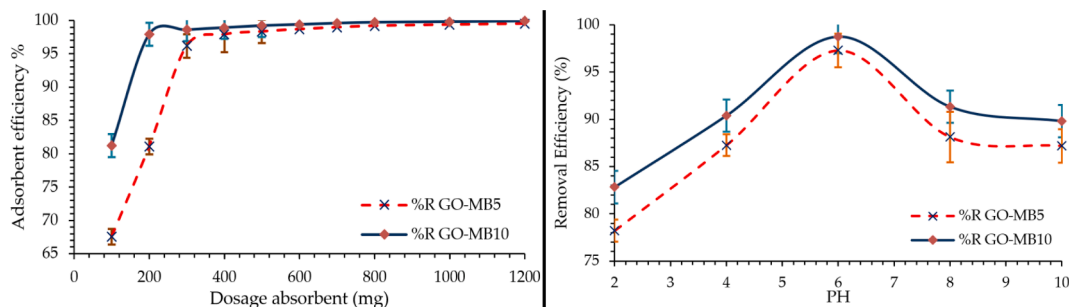


Fig. 7. Effect of (a) adsorbent dosage, (b) pH value on the adsorption efficiency of phenol onto adsorbents (at  $C_o = 100$  ppm, 8 h., 120 rpm, and  $25^\circ\text{C}$ ).

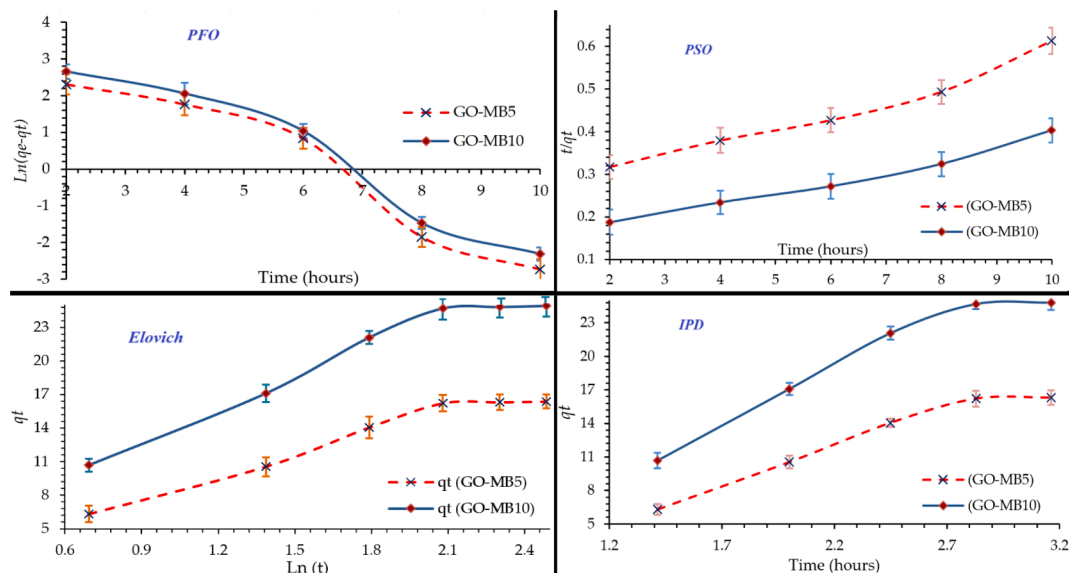


Fig. 8. Kinetic adsorption models for the phenol with error bars at ( $25^\circ\text{C}$ , 120 rpm,  $C_o = 100$  ppm, and pH 6).

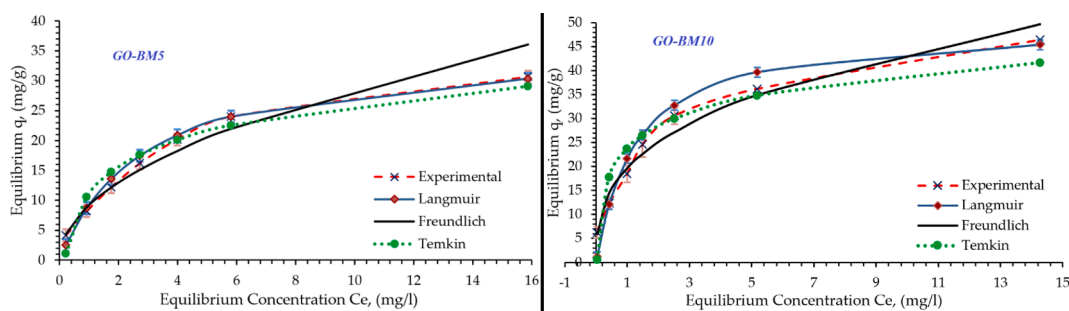


Fig. 9. Experimental and theoretical adsorption isotherms models for the phenol with error bars at ( $25^\circ\text{C}$ , 120 rpm, 8 h, and pH 6).

sites and their various binding strengths.

$$q_e = K_F C_e^{1/n} \tag{12}$$

$$\log q_e = \log K_F + 1/n \log C_e \tag{13}$$

where  $K_F$  is the Freundlich constant related to the sorption capacity, while  $1/n$  shows the sorption intensity.

The Temkin isotherm can be written in the following form [13]:

$$q_e = RT/b(\ln A C_e) \tag{14}$$

$$q_e = (RT/b)\ln A + (RT/b)\ln C_e \tag{15}$$

$$B = RT/b \tag{16}$$

where  $B$  corresponds to the heat of adsorption,  $R$  is the ideal gas constant ( $8.314 \text{ J/mol/K}$ ),  $T$  (K) is the Absolute Temperature at  $298 \text{ K}$ ,  $b$  is the Temkin isotherm constant, and  $A$  (L/g) is the equilibrium binding constant corresponding to the maximum binding energy.

The parameters of each model and adsorbent have been determined from the nonlinear equations based on the experimental data in Table 3. The initial adsorption rates are high; this may be due to the availability of many vacant sites initially for adsorption and the presence of the functional groups to adsorb phenolate ( $\text{C}_6\text{H}_5\text{O}^-$ ) from an aqueous solution. After that, the adsorption sites have filled up, and the phenol solution concentration is decreased until equilibrium is reached. An

**Table 3**

Surface area, total pore volume, and mean pore diameter characterization of RB, MB, GO-MB5 and GO-MB10 Adsorbents by BET analysis.

Adsorbents	BET Surface Area (m <sup>2</sup> /g)	Total Pore Volume (cm <sup>3</sup> /g)	Mean Pore Diameter(nm)
RB	20.992	0.1046	19.936
MB	48.959	0.1745	14.255
GO	26.375	0.193	29.27
GO-MB5	163.026	0.215	5.275
GO-MB10	184.312	0.238	5.165

obvious increase in the adsorption capacities from 16.90, 30.69 to 46.43 mg/g for MB, GO-MB5, and GO-MB10, respectively, due to the increases in surface area and pore volume, as well as functional groups that contributed to the growth of the adsorption capacity [1,11]. The results indicated that Langmuir isotherm is more in agreement with the experimental data than Freundlich and Tempkin adsorption isotherm for phenol removal onto all adsorbents depending on the values of the correlation coefficient R<sup>2</sup> [44] (see Table 4 and Table 5).

### 3.3. Desorption and reusability (stability)

Adsorption of adsorbed molecules from the adsorbent surface increases the reusability of the adsorbent. When the pH was equal to two, the adsorption of phenol was very low, according to the pH experiments. This means that at acidic pH, the adsorbed phenol molecules can be desorbed from the adsorbent. Based on these findings, phenol-loaded adsorbent was desorbed using 0.1 M HCl. The mixture was agitated for 6 h at 25 degrees Celsius before collecting, washing with distilled water, and drying the adsorbent for reuse in the next run. Fig. 10. even after six cycles, the adsorption capacity of GO-MB5 and GO-MB10 remained at least 85 % and 87 % of their initial values, respectively.

## 4. Conclusions

Treating wastewater is critical due to the environmental and human health risks it poses. The recovery process and restricted adsorption capacity of adsorbents, both attributed to organic contaminants, pose significant obstacles. Embarking on an innovative endeavor, this study sought to elevate activated bentonite (MB) for wastewater treatment by infusing it with graphene oxide (GO), crafted through Hummer's method. The collaboration birthed two remarkable phenol adsorbents—GO-MB5 and the standout performer, GO-MB10, showcasing an impressive 99.926 % phenol removal efficiency. The choreography of batch adsorption trials unveiled a captivating dance between adsorbent dosage and phenol elimination, reaching its crescendo at 0.3 g and 0.2 g for GO-MB5 and GO-MB10, respectively. These adsorbents showcased their prowess at the optimal pH of 6 and a constant temperature of 25 °C. In the kinetic arena, the experimental data harmonized with the Elovich model, surpassing the Intraparticle Diffusion model. Illuminating the

**Table 4**

The kinetic adsorption models constants for phenol remediation onto GO-MB5 and GO-MB10 adsorbents at 25 °C.

Model	Parameters	GO-MB5	GO-MB10
Pseudo first order Equation (4)	K1	0.6854	0.6727
	R <sup>2</sup>	0.9373	0.9494
Pseudo-second order Equation (6)	K2	0.005	0.0053
	R <sup>2</sup>	0.9661	0.9793
Elovich Equations (7) and (8)	α (mg/g.mint)	9.0857	16.24189
	β (g/mg)	0.16506	0.11775
	R <sup>2</sup>	0.9592	0.954
Intraparticle Diffusion Model Equation (9)	θ (mg/g)	-1.6855	-0.3028
	K <sub>id</sub> (mg/g.min <sup>0.5</sup> )	6.0606	8.5063
	R <sup>2</sup>	0.9574	0.947

**Table 5**

The isotherm constants of Langmuir, Freundlich, and Tempkin for phenol remediation onto GO-MB5 and GO-MB10 adsorbents at 25 °C.

Model	Parameters	GO-MB5	GO-MB10
Langmuir	Q <sub>0</sub> (mg/g)	35.8423	49.505
	K <sub>L</sub> (l/mg)	0.3483	0.78
	R <sup>2</sup>	0.988	0.9874
Freundlich	1/n	0.4945	0.348
	K <sub>f</sub>	9.1876	19.7015
	R <sup>2</sup>	0.9801	0.9798
Tempkin	A <sub>T</sub> (L/g)	5.5075	33.7954
	b <sub>T</sub>	381.1884	367.298
	B(J/mole)	6.4996	6.7454
	R <sup>2</sup>	0.9453	0.90

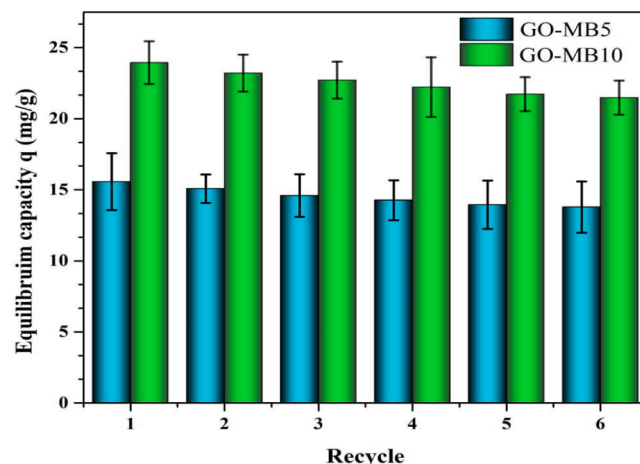


Fig. 10. Adsorption-reaeration cycles of GO-MB5 and GO-MB10 for phenol removal.

secrets of sorption, the Langmuir isotherm emerged as the belle of the ball, gracefully aligning with the experimental data and outshining the Freundlich and Tempkin models. As time unfolded, the phenol adsorption efficiency unveiled a gradual crescendo until equilibrium, donning its crown at the enchanting 8-hour mark for both GO-MB5 and the shining star, GO-MB10. Furthermore, their reusability without noticeable capacity loss gives them significant potential for practical application in phenol removal from water. In summary, this study highlights the importance of GO loading, contact time, pH, and isotherm models in enhancing adsorption and reveals GO-modified activated bentonite's improved adsorption capacity for phenol removal.

Future research might look at the temperature ranges, and whether they can be used to remove additional contaminants. The synthesis method might be optimized to increase adsorption capacities and efficiency, and potential scale-up strategies for real-world wastewater treatment applications could also be explored in additional research.

### CRedit authorship contribution statement

**Hassan Wathiq Ayoob:** Investigation, Resources. **Ali M. Ridha:** Software, Validation, Visualization. **Ala'a Abdulrazaq Jassim:** Data curation, Formal analysis, Writing – original draft. **Nabil Kadhim Taieh:** Data curation, Funding acquisition, Resources. **Raad Z. Homod:** . **Hayder Ibrahim Mohammed:** Conceptualization, Investigation, Writing – review & editing.

### Declaration of competing interest

The authors declare that they have no known competing financial interests or personal relationships that could have appeared to influence

the work reported in this paper.

## Data availability

No data was used for the research described in the article.

## References

- N.T. Abdel-Ghani, G.A. El-Chaghaby, F.S. Helal, Individual and competitive adsorption of phenol and nickel onto multiwalled carbon nanotubes, *J. Adv. Res.* 6 (3) (2015) 405–415, <https://doi.org/10.1016/j.jare.2014.06.001>.
- R.O. Ajemba, Structural alteration of Bentonite from Nkaliki by acid treatment: studies of the Kinetics and Properties of the modified samples, *Int. J. Adv. Eng. Technol.* 7 (1) (2014) 379–392.
- S. Al-Asheh, F. Banat, L. Abu-Aitah, Adsorption of phenol using different types of activated bentonites, *Sep. Purif. Technol.* 33 (1) (2003) 1–10, [https://doi.org/10.1016/S1383-5866\(02\)00180-6](https://doi.org/10.1016/S1383-5866(02)00180-6).
- M.A. Al-Ghouti, et al., Effective removal of phenol from wastewater using a hybrid process of graphene oxide adsorption and UV-irradiation, *Environ. Technol. Innov.* 27 (2022), 102525, <https://doi.org/10.1016/j.eti.2022.102525>.
- A.J. Amalanathan, et al., Impact of adding activated bentonite to thermally aged ester-based TiO<sub>2</sub> nanofluids on insulation performance, *IET Nanodielectrics* 4 (2) (2021) 63–74, <https://doi.org/10.1049/nde2.12010>.
- T.S. Anirudhan, M. Ramachandran, Removal of 2,4,6-trichlorophenol from water and petroleum refinery industry effluents by surfactant-modified bentonite, *J. Water Process Eng.* 1 (2014) 46–53, <https://doi.org/10.1016/j.jwpe.2014.03.003>.
- M.O. Ansari, et al., Anion selective pTSA doped polyaniline@graphene oxide-multiwalled carbon nanotube composite for Cr(VI) and Congo red adsorption, *J. Colloid Interface Sci.* 496 (VI) (2017) 407–415, <https://doi.org/10.1016/j.jcis.2017.02.034>.
- B. Paulchamy, G. Arthi, B.D. Lignesh, A simple approach to stepwise synthesis of graphene oxide nanomaterial, *J. Nanomed. Nanotechnol.* 06 (01) (2015) 1–4, <https://doi.org/10.4172/2157-7439.1000253>.
- S. Bendou, M. Amrani, Effect of hydrochloric acid on the structural of sodic-bentonite clay, *J. Miner. Mater. Charact. Eng.* 02 (05) (2014) 404–413, <https://doi.org/10.4236/jmmce.2014.25045>.
- H.N. Catherine, et al., Adsorption mechanism of emerging and conventional phenolic compounds on graphene oxide nanoflakes in water, *Sci. Total Environ.* 635 (2018) 629–638, <https://doi.org/10.1016/j.scitotenv.2018.03.389>.
- I.H. Dakhil, Removal of phenol from industrial wastewater using sawdust, *Res. Inventy: Int. J. Eng. Sci.* 3 (1) (2013) 25–31.
- M.A.L. Dutra, et al., Phenol removal from wastewater using eco-friendly hybrid hydrogels, *J. Appl. Polym. Sci.* 138 (30) (2021) 1–7, <https://doi.org/10.1002/app.50725>.
- U.A. Edet, A.O. Ifelebuegu, Wastewater using recycled brick waste, *Processes* 8 (665) (2020).
- B. Galindo, et al., Effect of the number of layers of graphene on the electrical properties of TPU polymers, *IOP Conf. Ser.: Mater. Sci. Eng.* 64 (1) (2014), <https://doi.org/10.1088/1757-899X/64/1/012008>.
- A. Gholampour, et al., Revealing the dependence of the physiochemical and mechanical properties of cement composites on graphene oxide concentration, *RSC Adv.* 7 (87) (2017) 55148–55156, <https://doi.org/10.1039/c7ra10066c>.
- W.S. Hummers, R.E. Offeman, Preparation of graphitic oxide, *J. Am. Chem. Soc.* 80 (6) (1958) 1339, <https://doi.org/10.1021/ja01539a017>.
- O. Idoko, et al., Adsorption of heavy metals (lead ion) from industrial waste water using acidified bentonite clay, *Int. J. Eng. Appl. Sci. Technol.* 04 (04) (2019) 394–401, <https://doi.org/10.33564/ijeast.2019.v04i04.063>.
- A.A. Inyibor, F.A. Adekola, G.A. Olatunji, Kinetics, isotherms and thermodynamic modeling of liquid phase adsorption of Rhodamine B dye onto *Raphia hookeri* fruit epicarp, *Water Resources Ind.* 15 (2016) 14–27, <https://doi.org/10.1016/j.wri.2016.06.001>.
- S.J. Kulkarni, et al., Adsorption of phenol from wastewater in fluidized bed using coconut shell activated carbon, *Proc. Eng.* 51 (NUICON 2012) (2013) 300–307, <https://doi.org/10.1016/j.proeng.2013.01.040>.
- M. De La Luz-Asunción, et al., Adsorption of phenol from aqueous solutions by carbon nanomaterials of one and two dimensions: kinetic and equilibrium studies, *J. Nanomater.* 2015 (2015), <https://doi.org/10.1155/2015/405036>.
- J.M. Li, et al., Adsorption of phenol, p-chlorophenol and p-nitrophenol onto functional chitosan, *Bioresour. Technol.* 100 (3) (2009) 1168–1173, <https://doi.org/10.1016/j.biortech.2008.09.015>.
- H. Liu, et al., Novel graphene oxide/bentonite composite for uranium(VI) adsorption from aqueous solution, *J. Radioanal. Nucl. Chem.* 317 (3) (2018) 1349–1360, <https://doi.org/10.1007/s10967-018-5992-0>.
- J. Liu, et al., U(VI) adsorption onto cetyltrimethylammonium bromide modified bentonite in the presence of U(VI)-CO<sub>3</sub> complexes, *Appl. Clay Sci.* 135 (2017) 64–74, <https://doi.org/10.1016/j.clay.2016.09.005>.
- B. Lou, et al., Solubility measurement and molecular simulation of unsolvated and solvated estrogen receptor agonist (R)-equol in binary solvents (alcohols + n-heptane) from 273.15 K to 333.15 K, *J. Mol. Liq.* 376 (2023), 121460, <https://doi.org/10.1016/j.molliq.2023.121460>.
- Y. Ma, et al., Removal of phenol by powdered activated carbon adsorption, *Front. Environ. Sci. Eng.* 7 (2) (2013) 158–165, <https://doi.org/10.1007/s11783-012-0479-7>.
- A. Mara, et al., Effect of sulfuric acid concentration of bentonite and calcination time of pillared bentonite, *AIP Conf. Proc.* 1725 (2016), <https://doi.org/10.1063/1.4945496>.
- K.M. Sahari, Dynamic indoor thermal comfort model identification based on neural computing PMV index, in: *IOP Conf. Ser.: Earth Environ. Sci.* 16, IOP Publishing, 2013, p. 012113, <https://doi.org/10.1088/1755-1315/16/1/012113>.
- P. Montes-Navajas, et al., Surface area measurement of graphene oxide in aqueous solutions, *Langmuir* 29 (44) (2013) 13443–13448, <https://doi.org/10.1021/la4029904>.
- D.M. Naguib, N.M. Badawy, Phenol removal from wastewater using waste products, *J. Environ. Chem. Eng.* 8 (1) (2020), 103592, <https://doi.org/10.1016/j.jece.2019.103592>.
- J.R. Palembang-prabumulih, O. Ilir, ADSORPTION OF PHENOL POLLUTANTS FROM AQUEOUS SOLUTION USING Ca-BENTONITE/CHITOSAN COMPOSITE (Adsorpsi Polutan Fenol dari Larutan Berair Menggunakan Komposit Ca-Bentonit/Kitosan) Poedji Loekitowati Hariani\* Fatma, Fahma Riyanti and Hesti Ratnasar, 22 (2) (2015) 233–239.
- R.Z. Homod, et al., Empirical correlations for mixed convection heat transfer through a fin array based on various orientations, *Int. J. Therm. Sci.* 137 (2019) 627–639, <https://doi.org/10.1016/j.ijthermalsci.2018.12.012>.
- V.H. Pham, et al., Chemical functionalization of graphene sheets by solvothermal reduction of a graphene oxide suspension in N-methyl-2-pyrrolidone, *J. Mater. Chem.* 21 (10) (2011) 3371–3377, <https://doi.org/10.1039/c0jm02790a>.
- H. Rahimzadeh, et al., Potential of acid-activated bentonite and SO<sub>3</sub>H-functionalized MWCNTs for biodiesel production from residual olive oil under biorefinery scheme, *Front. Energy Res.* 6 (DEC) (2018) 1–10, <https://doi.org/10.3389/fenrg.2018.00137>.
- J. Rojas, et al., Kinetics, isotherms and thermodynamic modeling of liquid phase adsorption of crystal violet dye onto shrimp-waste in its raw, pyrolyzed material and activated charcoals, *Appl. Sci. (Switzerland)* 9 (24) (2019), <https://doi.org/10.3390/app9245337>.
- H.H. Shaarawy, et al., Adsorption performance of coated bentonite via graphene oxide, *Bull. Natl. Res. Centre* 44 (1) (2020), <https://doi.org/10.1186/s42269-020-00299-8>.
- S.F.A. Shattar, N.A. Zakaria, K.Y. Foo, One step acid activation of bentonite derived adsorbent for the effective remediation of the new generation of industrial pesticides, *Sci. Rep.* 10 (1) (2020) 1–13, <https://doi.org/10.1038/s41598-020-76723-w>.
- V. Srihari, A. Das, Adsorption of phenol from aqueous media by an agro-waste (*Hemidesmus indicus*) based activated carbon, *Appl. Ecol. Environ. Res.* 7 (1) (2009) 13–23, [https://doi.org/10.15666/aer/0701\\_013023](https://doi.org/10.15666/aer/0701_013023).
- M.R. Thalji, et al., Solvothermal synthesis of reduced graphene oxide as electrode material for supercapacitor application nanomaterials for energy storage applications view project nonlinear modeling view project solvothermal synthesis of reduced graphene oxide as electrode, *Chem. Adv. Mater.* 4 (3) (2019) 17–26, <https://www.researchgate.net/publication/337945812>.
- L.G.C. Villegas, et al., A short review of techniques for phenol removal from wastewater, *Curr. Pollut. Rep.* 2 (3) (2016) 157–167, <https://doi.org/10.1007/s40726-016-0035-3>.
- J. Wei, et al., Graphene oxide-supported organo-montmorillonite composites for the removal of Pb(II), Cd(II), and As(V) contaminants from water, *ACS Appl. Nano Mater.* 3 (1) (2020) 806–813, <https://doi.org/10.1021/acsnano.9b02311>.
- W. Xu, et al., Fabrication of graphene oxide/bentonite composites with excellent adsorption performances for toluidine blue removal from aqueous solution, *Adv. Powder Technol.* 30 (3) (2019) 493–501, <https://doi.org/10.1016/j.apt.2018.11.028>.
- N.H. Yarkandi, Removal of lead (II) from waste water by adsorption, *Int. J. Curr. Microbiol. App. Sci.* 3 (4) (2014) 207–228.
- N. Yildiz, Z. Aktas, A. Calimli, Sulphuric acid activation of a calcium bentonite, *Part. Sci. Technol.* 22 (1) (2004) 21–33, <https://doi.org/10.1080/02726350490422392>.
- M. Yin, Y. Pan, C. Pan, Adsorption properties of graphite oxide for Rhodamine B, *Micro Nano Lett.* 14 (11) (2019) 1192–1197, <https://doi.org/10.1049/mnl.2018.5820>.
- L. Yu, et al., Removal of phenols from aqueous solutions by graphene oxide nanosheet suspensions, *J. Nanosci. Nanotechnol.* 16 (12) (2016) 12426–12432, <https://doi.org/10.1166/jnn.2016.12974>.
- C. Zhang, et al., Preparation of graphene oxide-montmorillonite nanocomposite and its application in multiple-pollutants removal from aqueous solutions, *Water Sci. Technol.* 79 (2) (2019) 323–333, <https://doi.org/10.2166/wst.2019.046>.
- S. Zhang, et al., Measuring the specific surface area of monolayer graphene oxide in water, *Mater. Lett.* 261 (2020), 127098, <https://doi.org/10.1016/j.matlet.2019.127098>.
- L. Zhirong, M. Azhar Uddin, S. Zhanxue, FT-IR and XRD analysis of natural Na-bentonite and Cu(II)-loaded Na-bentonite, *Spectrochim. Acta - Part A: Mol. Biomol. Spectrosc.* 79 (5) (2011) 1013–1016, <https://doi.org/10.1016/j.saa.2011.04.013>.